Central Asian Journal of Environmental Science and Technology Innovation **1** (2021) 12–19

RESEARCH PAPER

Fullerene (C_{20}) as a potential adsorbent and sensor for the removal and detection of picric acid contaminant: A DFT Study

Mohammad Reza Jalali Sarvestani [1]*, Pouya Charehjou[2]

[1] Young Researchers and Elite Club, Yadegar-e-Imam Khomeini (RAH) Shahr-e-Rey Branch, Islamic Azad University Tehran, Iran

[2] Pazhohehsaraye aknar sarabi.st;shahid montazeri.Tabriz Iran

Highlights

- The adsorption of picric acid on the surface of C_{20} fullerene is explored using DFT calculations.
- HUMO/LUMO bandgap of C_{20} reduces significantly in the adsorption process.
- Picric acid desorbs from the adsorbent surface by increasing of temperature.

Graphical Abstract

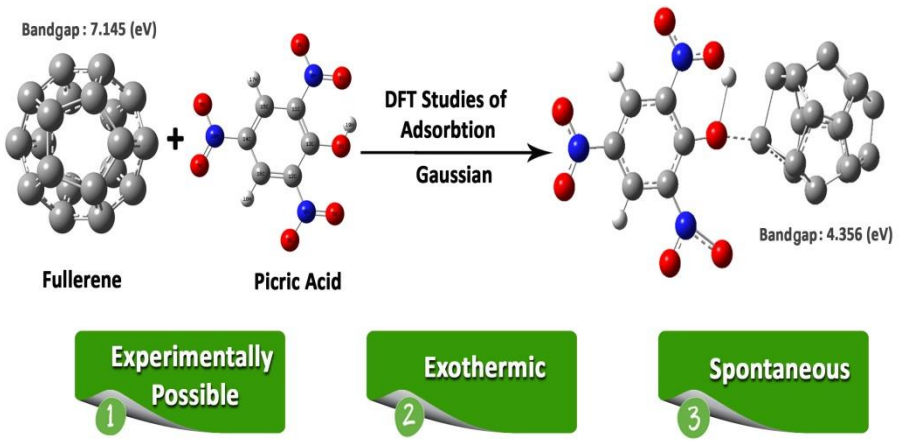

Article Info

Receive Date: 29 December 2020
Revise Date: 19 January 2020
Accept Date: 28 January 2020
Available online: 10 February 2020

Keywords:
Adsorption
Picric acid
Fullerene (C_{20})
Density functional theory

Abstract

Picric acid is a nitrophenol environmental contaminant that has adverse effects on the environment and the health of humans. Therefore, its removal and detection are very important. In this respect, infra-red (IR), natural bond orbital (NBO) and frontier molecular orbital (FMO) computations were employed for estimating the performance of fullerene (C_{20}) as a sensor and adsorbent for picric acid. The calculated values of adsorption energy, Gibbs free energy changes and enthalpy variations showed picric acid adsorption on the surface of fullerene is experimentally possible, exothermic and spontaneously. In the adsorption process, the specific heat capacity of fullerene increased from 152.495 to 361.224 J/Mol.K but its bandgap declined -39.039% from 7.145 (eV) to 4.356 (eV) that indicated the thermal and electrical conductivity of fullerene enhanced remarkably when picric acid was adsorbed on its surface and this nanostructure is a suitable sensing material for the construction of new thermal and electrochemical sensors. The influence of temperature was also checked out and the results showed picric acid interaction with C_{20} was more favorable in lower temperatures. The NBO computations showed picric acid interaction with fullerene was chemisorption. The FMO results showed the chemical hardness of picric declined after its interaction with fullerene and picric acid-C_{20} complexes were more reactive than pure picric acid. The electrophilicity and maximum transferred charge capacity indices demonstrated the tendency of picric acid towards electron decreased after it was adsorbed on the surface of fullerene and picric acid-fullerene complexes were less electrophile than pure picric acid. Other structural parameters were also discussed in detail.

10.22034/CAJESTI.2021.01.02

E-ISSN: 2717-0519
P-ISSN: 2717-4034

* Corresponding author: Rezajalali93@yahoo.com (M.R. Jalali Sarvestani)

1. Introduction

Picric acid (PA, Fig. 1) is a nitrophenol environmental contaminant that is widely used in various industries such as the production of explosives, fireworks, leather, plastics, dyes and medicinal compounds and consequently its discharge to the environment is highly probable (Dennie et al., 1929; Parham et al., 2012). The former researches showed, even short term exposure to PA can lead to serious health problems like Hepatitis, dizziness, headaches, jaundice, diarrhea, different types of cancer, hemorrhagic nephritis, discomfort, respiratory distress and gastroenteritis in humans and other living organisms (Huang et al., 2014; Nipper et al., 2005). In this respect, developing new effective methods for the removal and detection of PA is of great importance (Song et al., 2019). To date, different methods including filtration, oxidation/precipitation, adsorption, photocatalytic degradation, electrochemical destruction, ozonization, aerobic and anaerobic biological treatment, coagulation/flocculation and reverse osmosis have been reported for the removal of environmental pollutants (Doroudi and Jalali Sarvestani, 2020). However, in the mentioned techniques, adsorption is more preferable because of being economical, easy operability, rapidness, flexibility and high efficiency (Agarwal et al., 2014). But, the main challenge for the adsorption method is finding an economical adsorbent with high adsorption capacity, good selectivity, enough reusability and applicability in harsh conditions (Uslu and Demir, 2010). Furthermore, various analytical techniques such as capillary electrophoresis, fluorimetry, UV-Visible spectrophotometry, high-performance liquid chromatography, mass spectrometry and gas chromatography have been reported for the measurement of PA but all of the referred methods are expensive, time-consuming and demanding large amounts of toxic organic solvents (Mahyari, 2016; Wang et al., 2018; Huang et al., 2014). In addition, highly experienced operators are needed for implementing the complicated sample-pretreatment steps before the main analysis process (Mohseni Kafshgari and Tahermansouri, 2017). On the other hand, thermal and electrochemical sensors are prominent alternatives for the mentioned analytical techniques because these types of sensors are small, portable and economical devices that can be also applied in colored and opaque specimens (Rashvand et al., 2020).

Simple instrumentation, high selectivity and sensitivity, rapid analysis time and wide linear range are other advantages of thermal and electrochemical sensors. However, the first step in developing a new sensor for the determination of an analyte is selecting an appropriate sensing material that interacts selectively with the desired analyte and this interaction should lead to a substantial difference in the electrical or thermal conductivity of the sensing material (Rashvand et al., 2020). On the other hand, fullerene (C_{20}), is the smallest nanomaterial with a dodecahedral cage structure (Fig. 1). The structure of this fullerene is highly curved and it is composed of pentagonal rings (Jalali Sarvestani and Ahmadi, 2020). C_{20} has unique traits that make it an eminent sensing material like high conductance, great surface area/ volume ratio and excellent reactivity (Jalali Sarvestani and Doroudi, 2020). In this respect, the goal of this study is to evaluate the performance of C_{20} as an adsorbent and a sensor for removal and detection of PA by density functional theory simulations.

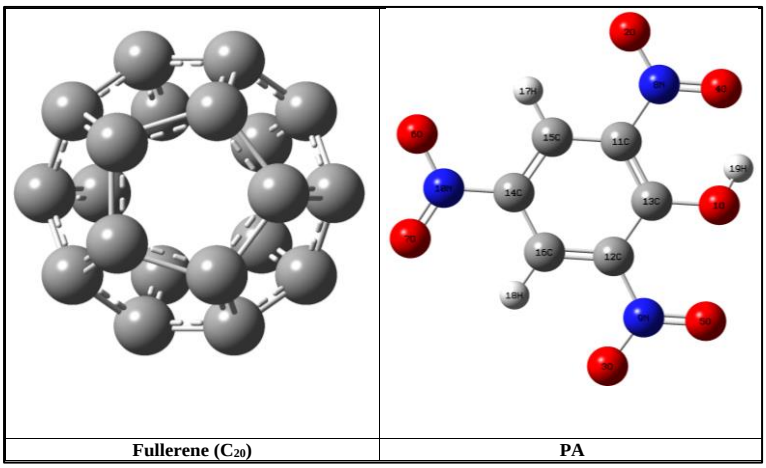

Fig. 1. The optimized structures of C_{20} and PA.

2. Materials and Methods

The structures of C_{20}, PA and their complexes were designed by Nanotube modeler 1.3.0.3 and Guass View 6 softwares. Firstly, all of the designed structures were optimized geometrically. Then, IR, NBO and FMO computations were done on them. All of the computations were performed by Gaussian 16 software using the density functional theory method in the B3LYP/6-31G (d) level of theory. This level of theory was chosen because in previous works its results were in admissible accordance with the experimental data. Guass Sum 3.0 software was used for obtaining the density of states (DOS) spectrums. All of the computations were done in the aqueous phase in the temperature range of 298-398 K at 10° intervals.
The studied processes were as follows:

PA + Adsorbent ⟶ PA-Adsorbent (1)

Equations 2-5 were used for calculating adsorption energy values (E_{ad}) and thermodynamic parameters including adsorption enthalpy changes (ΔH_{ad}), Gibbs free energy changes (ΔG_{ad}) and thermodynamic equilibrium constant (K_{th}) respectively.

$$E_{ad} = \left(E_{(\text{PA-Adsorbent})} - \left(E_{(\text{PA})} + E_{(Adsorbent)} + E_{(BSSE)}\right)\right) \quad (2)$$

$$\Delta H_{ad} = \left(H_{(\text{PA-Adsorbent})} - \left(H_{(\text{PA})} + H_{(Adsorbent)}\right)\right) \quad (3)$$

$$\Delta G_{ad} = \left(G_{(\text{PA-Adsorbent})} - \left(G_{(\text{PA})} + G_{(Adsorbent)}\right)\right) \quad (4)$$

$$K_{th} = \exp\left(-\frac{\Delta G_{ad}}{RT}\right) \quad (5)$$

In the aforementioned equations, E is the total electronic energy of each structure, E_{BSSE} is the basis set superposition correction, H denotes the sum of the thermal correction of enthalpy and total energy of the evaluated materials. The G stands for the sum of the thermal correction of Gibbs free energy and total energy for each of the studied structures. R denotes the ideal gas constants and T stands for the temperature (Rashvand et al., 2020). Frontier molecular orbital parameters including bandgap (E_g), chemical hardness (η), chemical potential (μ), electrophilicity (ω) and the maximum charge capacity (ΔN_{max}) were calculated by equations 6-11.

$$\text{Eg} = E_{LUMO} - E_{HOMO} \quad (6)$$

$$\%\Delta\text{Eg} = \frac{Eg2 - Eg1}{Eg1} \times 100 \quad (7)$$

$$\eta = {}^{(E_{LUMO} - E_{HOMO})}/_{2} \quad (8)$$

$$\mu = {}^{(E_{LUMO} + E_{HOMO})}/_{2} \quad (9)$$

$$\omega = {}^{\mu^2}/_{2\eta} \quad (10)$$

$$\Delta N_{max} = -{}^{\mu}/_{\eta} \quad (11)$$

E_{LUMO} and E_{HOMO} in equations 6 to 11 are the energy of the lowest unoccupied molecular orbital and the energy of the highest occupied molecular orbital respectively. E_{g1} and E_{g2} are the bandgaps of the Nano-adsorbent and PA-Adsorbent complex respectively (Ahmadi and Jalali Sarvestani, 2020).

3. Results and Discussion

PA interaction with fullerene was scrutinized at two different modes to find the most stable configuration. The initial and optimized structure of PA-C_{20} complexes is given in Fig. 2. As can be seen, at A-Conformer,

fullerene is inserted in parallel form towards the benzene ring of PA and at B-Conformer, the nanostructure is placed near the nitro and hydroxyl functional groups of the adsorbate. As it is clear from Fig. 2, sharp structural deformations have occurred after geometrical optimizations at both conformers that can be due to the formation of chemical bonds between PA and C_{20}. The calculated values of total electronic energy, adsorption energy, zero-point energy (ZPE), the minimum and maximum IR frequencies and dipole moment for both investigated configurations are given in Table 1. As can be observed, B-Conformer is more energetically stable than A-Conformer because it has a lower total electronic energy. Besides, the adsorption energy is considerably negative for both configurations indicating that the adsorption process is experimentally possible (Rashvand et al., 2020).

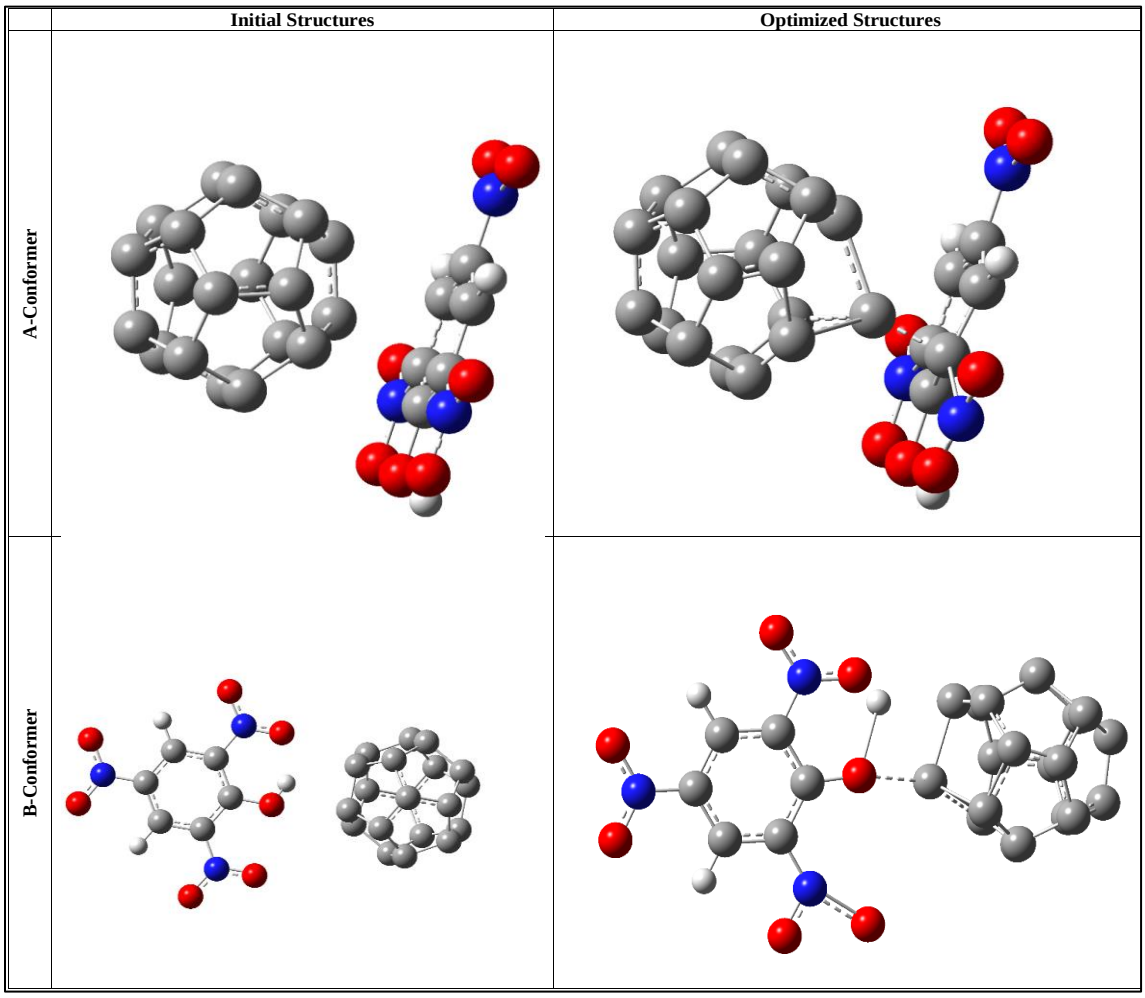

Fig. 2. Initial and optimized structures of PA-C_{20} complexes.

The computed minimum and maximum IR frequencies revealed all of the evaluated structures are a true local minimum because there was not observed any negative frequency. The dipole moment of PA increased sharply from 2.620 to 8.440 and 7.430 for A and B conformers respectively after it was adsorbed on the surface of C_{20} indicating that the reactivity of PA enhanced significantly after its interaction with fullerene. In order to obtain more information about the adsorption mechanism, NBO calculations were also implemented on the optimized structure and the results are tabulated at Table 2. As can be observed, a two-electron containing monovalent chemical bond with SP3 hybridization is created between adsorbate and adsorbent at both configurations. Hence, PA interaction with C_{20} is chemisorption (Ahmadi and Jalali Sarvestani, 2020).

Table 1. Structural properties of PA, C_{20} and their complexes.

NO	Total electronic energy (a.u)	Ead (kJ/mol)	ZPE (kJ/mol)	νmin (cm^{-1})	νmax (cm^{-1})	Dipole Moment (Deby)
PA	-903.854	---	321.250	51.190	3722.739	2.620
C_{20}	-747.196	---	325.260	261.392	1690.640	0.000
A-Conformer	-1651.098	-74.722	672.290	0.977	3722.867	8.440
B-Conformer	-1651.120	-132.483	672.220	0.927	3722.612	7.430

Table 2. NBO results for PA-C_{20} complexes.

NO	Chemical bonds	Bond energy (a.u)	Hybridization	Occupancy	Bond order	Bond length (Å)
A-Conformer	C_{11}-C	-0.096	$SP^{2.99}$	1.98	1	1.566
B-Conformer	O_1-C	-0.106	$SP^{3.04}$	2.03	1	1.921

The thermodynamic parameters of the adsorption process were also calculated and the results are presented as a function of temperature at Fig. 3. As can be seen, the ΔHad values are negative for both conformers implying the adsorption procedure is exothermic. The influence of temperature on ΔHad was also studied and the results showed temperature does not have a tangible impact on this parameter. The CV of fullerene increased remarkably after adsorption of PA on its surface indicating the thermal conductivity of C_{20} improved substantially in the adsorption process and this nanostructure can be used as a sensing material for the construction of thermal sensors for detection of PA. In a thermal sensor, a recognition element (here C_{20}) is stabilized on the surface of a sensitive thermistor then the desired analyte should have a highly exothermic or endothermic interaction with the recognition element and the changes in the temperature of the sensor microenvironment temperature will be measure by the sensitive thermistor and it will be used as a signal that has a direct relationship with the analyte concentration (Jalali Sarvestani and Ahmadi, 2020). The negative values of ΔGad demonstrated that PA interaction with fullerene is spontaneous. The values of Kth indicating the adsorption process is more favorable and irreversible at lower temperatures but by increasing of temperature the adsorption becomes more reversible.

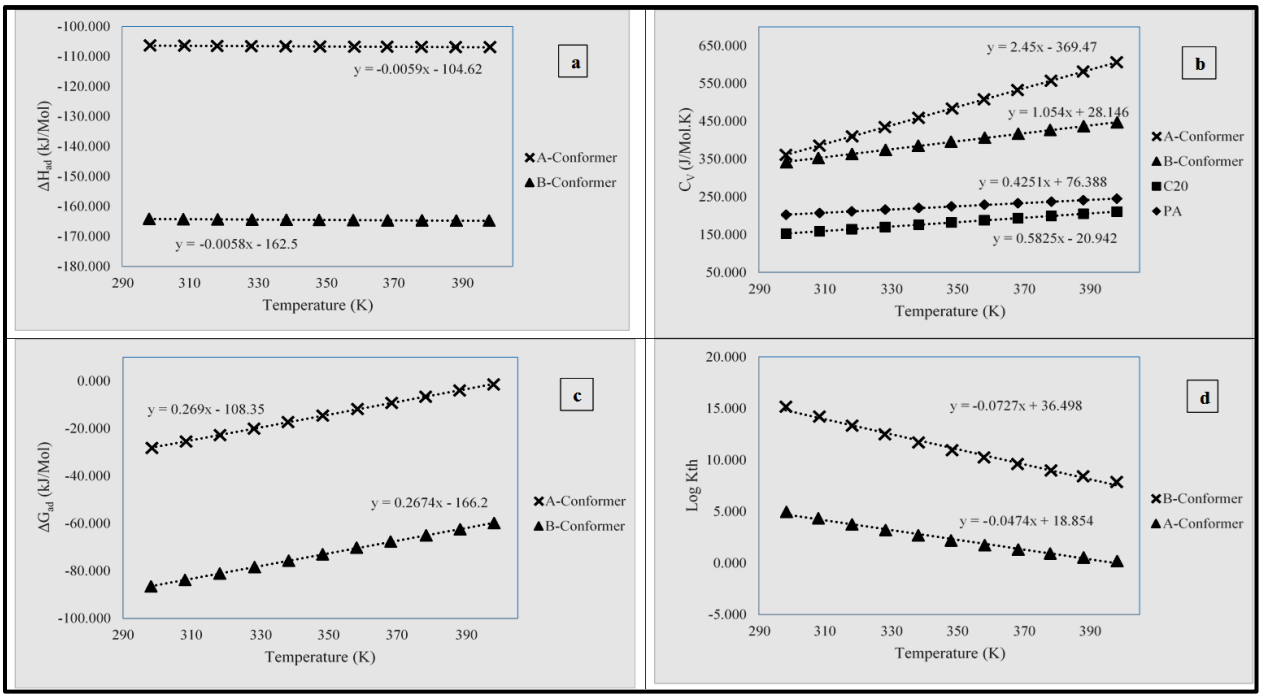

Fig. 3. The calculated thermodynamic parameters including ΔH_{ad}, C_V, ΔG_{ad} and Log K_{th} in temperature range of 298.15-398.15 at 10° intervals.

For investigating the capability of Fullerene as an electroactive sensing material, the DOS spectrums of PA, C_{20} and their complexes were computed and the results are presented at Fig. 4. As can be observed, the bandgap of fullerene is 7.145 (eV) but when PA adsorbs on its surface, Eg declines -29.199 and 39.039% to 5.059 and 4.356 (eV) for A and B conformers respectively. Bandgap has an inverse relationship with electrical conductivity. In fact, compounds with narrow bandgap are more conductive than materials with wider bandgap (Ahmadi and Jalali Sarvestani, 2020). Therefore, it can be deduced that the electrical conductivity of fullerene enhanced in its interaction process with PA and C_{20} is an excellent sensing material for the fabrication of new electrochemical sensors for the detection of PA (Jalali Sarvestani and Ahmadi, 2020).

Other frontier molecular orbital parameters including chemical hardness, chemical potential, electrophilicity and maximum transferred charge capacity were also calculated and the results are given in Table 3. As can be seen, the chemical hardness of PA is 7.740 (eV) but when it adsorbs on the surface of fullerene, its chemical hardness decreases to 3.537 and 3.842 (eV) at A and B conformers. Therefore, PA-C_{20} complexes are more reactive and softer than pure PA without the nanostructure because the electron transmissions that are necessary for the implementation of chemical reactions can be done more conveniently in them. The calculated chemical potential values are negative for all of the structures indicating that the scrutinized structures are thermodynamically stable (Jalali Sarvestani and Doroudi, 2020).

When two molecules participate in a reaction, one of them acts as an electrophile and the other plays the role of a nucleophile. Electrophilicity and maximum transferred charge capacity are good standards for estimating the tendency of materials towards the electron. Indeed, the molecules with higher values of electrophilicity and lower amounts of ΔNmax are more electrophile than other molecules. As the provided data in Table 3, shows clearly when PA adsorbs on the surface of fullerene, the ω index decline from 5.165 to 2.529 and 2.178 (eV) while ΔNmax experiences a tangible increase from -2.575 to -1.008 and -1.664 (eV) at A and B conformers. Therefore, it can be inferred that PA-C_{20} complexes have less tendency towards electrons in comparison to pure PA without fullerene (Rashvand et al., 2020).

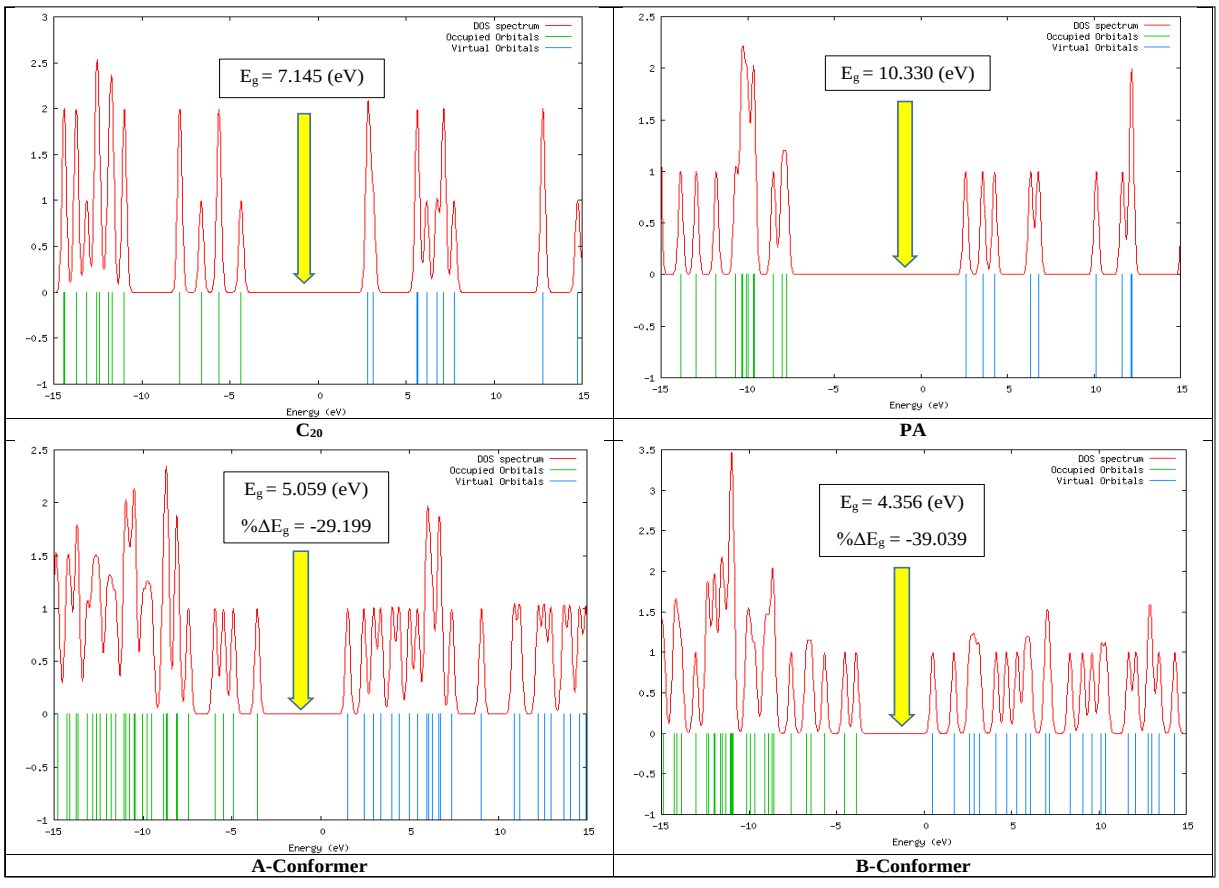

Fig. 4. DOS spectrums of PA, C_{20} and their complexes.

Table 3. Frontier molecular orbital parameters for PA, C_{20} and their complexes.

NO	E_{HOMO} (eV)	E_{LUMO} (eV)	E_g (eV)	$\%\Delta E_g$	η (eV)	μ (eV)	ω (eV)	ΔN_{max} (eV)
PA	-7.740	2.590	10.330	---	7.740	-2.590	5.165	-2.575
C_{20}	-4.323	2.822	7.145	---	3.573	-0.751	0.079	0.210
A-Conformer	-3.537	1.522	5.059	-29.199	3.537	-1.522	2.529	-1.008
B-Conformer	-3.842	0.513	4.356	-39.039	3.842	-0.514	2.178	-1.664

4. Conclusion

In this research, PA interaction with C_{20} was investigated using DFT computations. The calculated adsorption energies showed the adsorption process is experimentally feasible and the obtained thermodynamic parameters indicated PA interaction with fullerene is exothermic, spontaneous and more favorable in lower temperatures. The DOS spectrums showed when PA adsorbs on the surface of fullerene the bandgap decreases from 7.145 (eV) to 4.356 (eV), therefore, this nanostructure can be used as a promising electrochemical sensing material for the detection of PA. Besides, the sharp increase of specific heat capacity in the adsorption process of PA indicated thermal conductivity of fullerene enhanced when PA adsorbs on its surface and C_{20} can be employed for the development of new thermal sensors to PA detection. The NBO results showed PA interaction with C_{20} is chemisorption and fullerene is an appropriate adsorbent for the removal of PA from environmental specimens.

References

Agarwal, B., Mendez, R.G., Lanza, M., Sulzer, P., Mark, T.D., Thomas, N., Mayhew, C.A., 2014. Sensitivity and Selectivity of Switchable Reagent Ion Soft Chemical Ionization Mass Spectrometry for the Detection of Picric Acid. *J. Phys. Chem. A.*, **118**(37) 8229-8236. https://doi.org/10.1021/jp5010192

Ahmadi, R., Jalali Sarvestani, M.R., 2020. Adsorption of Tetranitrocarbazole on the Surface of Six Carbon-Based Nanostructures: A Density Functional Theory Investigation. *Russ. J. Phys. Chem. B.*, **14**(1), 198-208. https://doi.org/10.1134/S1990793120010194

Dennie, C.C., Mcbride, W.L., Davis, P.E., 1929. Toxic Reactions Produced By The Application Of Trinitrophenol (Picric Acid). *Arch. Derm. Syphilol.*, **20**(5), 698-704. https://doi.org/10.1001/archderm.1929.01440050108008

Doroudi, Z., Jalali Sarvestani, M.R., 2020. Boron nitride nanocone as an adsorbent and senor for Ampicillin: A Computational Study. *Chem. Rev. Lett.*, **3**(3), 110-116. https://dx.doi.org/10.22034/crl.2020.233274.1061

Huang, J., Wang, L., Shi, C., Dai, Y., Gu, C., Liu, J., 2014. Selective detection of picric acid using functionalized reduced graphene oxide sensor device. *Sens. Actuat. B. Chem.*, **196**, 567-573. https://doi.org/10.1016/j.snb.2014.02.050

Jalali Sarvestani, M.R., Doroudi, Z., 2020. Removal of Reactive Black 5 from Waste Waters by Adsorption: A Comprehensive Review. *J. Water. Environ. Nanotechnol.*, **5**(2), 180-190. https://dx.doi.org/10.22090/jwent.2020.02.008

Jalali Sarvestani, M.R., Ahmadi, R., 2020. Trinitroanisole Adsorption on the Surface of Boron Nitride Nanocluster (B12N12): A Computational Study. *J. Water Environ. Nanotechnol.*, **5**(1), 34-44.

Mahyari, M., 2016. Electrochemical determination of picric acid based on platinum nanoparticles–reduced graphene oxide composite. *Int. J. Environ. Anal. Chem.*, **96**(15), 1455-1468. https://doi.org/10.1080/03067319.2016.1268606

Mohseni Kafshgari, M., Tahermansouri, H., 2017. Development of a graphene oxide/chitosan nanocomposite for the removal of picric acid from aqueous solutions: Study of sorption parameters. *Colloids. Surf. B.*, **160**, 671-681. https://doi.org/10.1016/j.colsurfb.2017.10.019

Nipper, M., Carr, R.S., Biedenbach, J.M., Hooten, R.L., Miller, K., 2005. Fate and effects of picric acid and 2,6-DNT in marine environments: Toxicity of degradation products. *Mar. Pollut. Bull.*, **50**(11), 1205-1217. https://doi.org/10.1016/j.marpolbul.2005.04.019.

Parham, H., Zargar, B., Rezazadeh, M., 2012. Removal, preconcentration and spectrophotometric determination of picric acid in water samples using modified magnetic iron oxide nanoparticles as an efficient adsorbent. *Mater. Sci. Eng. C.*, **32**(7), 2109-2114. https://doi.org/10.1016/j.msec.2012.05.044

Rashvand, H.R., Hajiaghababaei, L., Darvich, M.R., Jalali Sarvestani, M.R., Jaberi Miyandoab, F., 2020. A Liquid Membrane Mercury Selective Electrode Based on 2-(N-pipyridino Methyl)-1-Cyano Cyclohexanol as a Novel Neutral Carrier. *J. Anal. Chem.*, **75**(10), 1340-1347. https://doi.org/10.1134/S106193482010010X

Song, Y.Z., Pang, X.J., Chen, J., Lu, Y.T., Xie, J., Ye, Y., 2019. Determination of picric acid using micro CdS crystal-modified glassy carbon electrode. *Int. J. Environ. Anal. Chem.*, **100**(9), 957-967. https://doi.org/10.1080/03067319.2019.1646257

Uslu, H., Demir, G., 2010. Adsorption of Picric Acid from Aqueous Solution by the Weakly Basic Adsorbent Amberlite IRA-67. *J. Chem. Eng. Data.*, **55**(9), 3290-3296. https://doi.org/10.1021/je100088u

Wang, M., Zhang, H., Guo, L., Gao, D., 2018. Fluorescent polymer nanotubes as bifunctional materials for selective sensing and fast removal of picric acid. *Sens. Actuat. B. Chem.*, **274**, 102-109. https://doi.org/10.1016/j.snb.2018.07.132

How to cite this paper:
Jalali Sarvestani, M.R., Charehjou, P., 2021. Fullerene (C_{20}) as a potential adsorbent and sensor for the removal and detection of picric acid contaminant: A DFT Study. *Cent. Asian J. Environ. Sci. Technol. Innov.*, **1**, 12-19.